MULTISCALE EXTENSIONS OF THE CELLULAR POTTS MODELS: TOWARD A NESTED-HYBRID APPROACH

Publisher copyright

(Article begins on next page)

04 August 2020

Multiscale extensions of the cellular Potts models: toward a nested-hybrid approach

Marco Scianna[1]

[1] *Dipartimento di Scienze Matematiche,*
Politecnico di Torino, Italy
marcosci1@alice.it

Communicated by Associated editor

Abstract

Multiscale problems are ubiquitous in all biological phenomena, which emerge from the complex interaction between processes happening at various levels. A number of mathematical approaches have been developed to address such an intricate network of organization. Among others, the cellular Potts model is particularly well-known and widespread. The CPM is a discrete, lattice-based, flexible technique able to accurately identify and describe the phenomenological mechanisms responsible for innumerable biological phenomena. This work discusses some innovative extensions of the method, whose aim is to increase its accuracy and to create a multilevel framework able to deal with the multiscale organization typical of biological development. Such CPM extensions are finally tested with sample applications, that show their potential and biological realism.

Keywords: `cellular Potts model, multiscale model, hybrid model.`

AMS Subject Classification: `92B05, 92C05, 92C17`

1. Introduction.

All biological phenomena emerge from the intricate interaction between multiple levels of organization: the molecular scale, the cell and the tissue. These natural levels can be approximately connected with, respectively, a microscopic, a mesoscopic and a macroscopic scale. In particular, the microscopic scale refers to those processes that occur at the subcellular level, such as DNA synthesis and duplication, activation of receptors, transduction of chemical signals and protein networks. The mesoscopic scale, on the other hand, can be referred to cell-level phenomena, such as cell duplication, death or motion. Finally, the macroscopic scale corresponds to those processes typical of the multicellular level, such as population reorganization, growth and dynamics. Such a multilevel flux of information is often too complex to be studied with only *experimental techniques*, which there-

fore need an increasing collaboration with *applied mathematics*. In fact, even though no hypothetically perfect single model can incorporate each and every process involved in the considered phenomenon, a computational approach is able to simplify the biological problem, offering both a concise description of its essential features, and to have a predictive power, determining the consequences of experimental manipulations.

Of the wide range of mathematical approaches, the class of *discrete* models represents one of the most suited for biological problems. Also called Individual Cell-Based Models (IBMs, for comprehensive reviews see [1,2]), they are typically focused on the cell-level of abstraction. Indeed, they represent biological cell-scale individuals as one or a set of discrete units, with rules describing their movements and interactions. In particular, the morphology of the elements is restricted according to some underlying discretization of the simulation domain, which can be either regular (such as square or cubic grids) or irregular (Voronoi tassellation). These approaches can be further classified into two categories: those for which each individual is correlated to a single spatial unit of the domain, and those for which each element can be formed by a collection of spatial units. IBMs can therefore naturally capture the biophysical properties of each individual, such as shape, movement or adhesion, and handle their interactions. In cell-based methods, the cell-scale elements behave according to a relatively small set of prescribed rules, which they execute depending on their type and on the signals they receive from the neighbors and from the environment. In particular, these techniques are able to analyze the mechanisms by which relatively simple behaviors and interactions of individuals collectively direct macroscopic pattern formation and development, and, vice versa, to infer how phenomena occurring at the macroscopic level feed back to the phenomenology of single elements.

In the last decades, purely discrete methods have been increasingly integrated with *continuous* approaches suited to describe the evolution of microscopic variables (i.e., ion or molecules). The aim is to create *hybrid* environments able to span both the mesoscopic and the microscopic scale with a sufficient level of accuracy, see as an example [3,4]. One of these computational environments is the Cellular Potts Model (CPM, also called Glazier-Graner-Hogeweg model developed in [5,6] and reviewed in [7,8]). As a generalization of the Ising model, the CPM is a grid-based, Monte Carlo method, whose core is an energy minimization philosophy, which drives the evolution of the simulated system.

In this paper, we present some important developments of the method, detailed in Sections 2 and 3. Test applications are then illustrated to show how the proposed model extensions can be applied to specific biological

problems with a significative accuracy and experimental usefulness. Finally, in the last part of the work, cf. Section 4, the conclusions are drawn.

2. Uncompartmentalized CPM.

All CPMs include a list of objects, a description of their interactions and rules for their dynamics. The CPM domains are d-dimensional lattices $\Omega \subseteq \mathbb{R}^d$, where $d = 1, 2, 3$. The term lattice defines a regular repeated graph, formed by identical d-dimensional closed grid sites $\mathbf{x} \in \mathbb{R}^d$, which therefore represent the basic unit of length of the system. Each site $\mathbf{x} \in \Omega$ is labeled by an integer number, $\sigma(\mathbf{x}) \in \mathbb{N}$, which can be interpreted as a degenerate spin coming from the original Ising approach [9,10]. The border of $\mathbf{x}$ is denoted by $\partial \mathbf{x}$, one of its neighbors by $\mathbf{x}'$, while its overall neighborhood by $\Omega'_{\mathbf{x}} = \{\mathbf{x}' \in \Omega : \mathbf{x}'$ is a neighbor of $\mathbf{x}\}$. Objects in the CPM are either *discrete* or *continuous*: this coexistence provides to the method its *hybrid* characteristic. Discrete objects Σ_σ are finite, spatially-extended lattice subdomains of contiguous sites denoted with the same spin σ, i.e. $\Sigma_{\overline{\sigma}} = \{\mathbf{x} \in \Omega : \sigma(\mathbf{x}) = \overline{\sigma}\}$. They are therefore undifferentiated *functional units* which, in basic CPMs, represent individual cell-scale elements (e.g., bacteria, unicellular organisms, single cells or ECM fibers). A collection of N discrete individuals Σ_σ is defined by N integer spins $\sigma = 1, 2, \ldots, N$, see Fig. 1. The borders between sites with different spins, that are thus shared between a couple of objects, define their membranes, i.e. $\partial \Sigma_\sigma = \bigcup_{\mathbf{x} \in \Sigma_\sigma, \mathbf{x}' \in \Omega'_{\mathbf{x}} : \mathbf{x}' \notin \Sigma_\sigma} (\partial \mathbf{x} \cap \partial \mathbf{x}')$. Each unit Σ_σ has a set of attributes (both geometrical, such as volume and surface, and biophysical, such as velocity and elasticity), and an associated type $\tau(\Sigma_\sigma)$ (e.g. endothelial cell, fibroblast, or ECM fiber). Mesoscopic, cell-level objects rearrange their boundaries to realistically reproduce shape changes and motion. Moreover, they can grow, die, duplicate and carry a set of possible rules for transitions between types.

Continuous objects, or *fields*, represent the spatio-temporal evolution of microscopic entities, that may reside within the discrete objects (e.g., DNA, RNA, cytosolic ions, or proteins), or in the external environment (e.g., growth factors, matrix proteins or matrix metallo-proteinases). They are described as variable concentrations with standard *reaction-diffusion* (RD) equations, which are numerically solved using *finite element schemes* on grids that exactly match the CPM domain and that are discretized at the same resolution. Specific interactions between discrete cell-level objects and continuous molecular-level objects can be characterized either by reaction terms in diffusion equations, as in the case of cell absorption and secretion of chemical diffusants, or, as we will explain hereafter, by constitutive laws
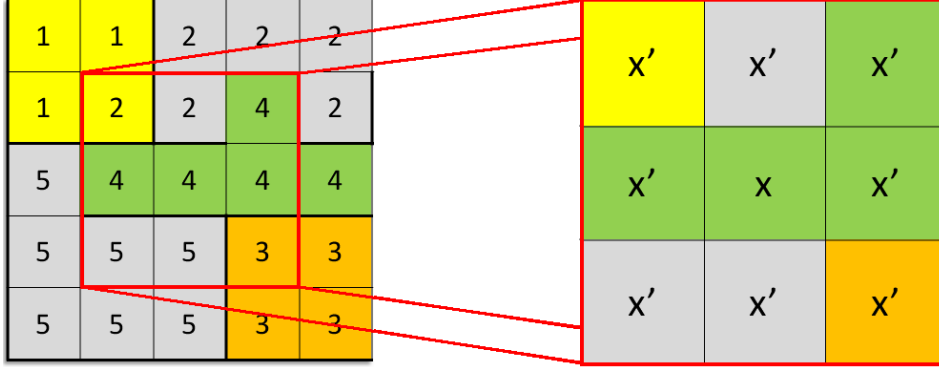
Figure 1. Typical 2D rectangular CPM lattice. The integer numbers (σ) identify single discrete objects. Individuals $\Sigma_{\sigma=2}$ and $\Sigma_{\sigma=5}$, identified by the same color, are of the same type τ. The zoom view shows a lattice site $\mathbf{x}$ and its overall neighborhood $\Omega'_{\mathbf{x}}$.

relating the mesoscopic properties of discrete individuals to the evolution of specific microscopic variables.

The CPM core principle consists of an iterative stochastic minimization of a system free energy, which is described by the *Hamiltonian functional* H, that will be defined in detail below. Simulated objects in fact rearrange to gradually reduce such a pattern energy. The minimization philosophy is implemented by modified version of the classical Metropolis algorithm for Monte Carlo-Boltzmann thermodynamics [6,11], evolving through repeated probabilistic updates of the site identification spins. Procedurally, at each time step, t, a lattice site $\mathbf{x}$, belonging to object Σ_σ, is randomly selected (*source voxel*), and proposed to copy its spin $\sigma(\mathbf{x})$ into an arbitrary unlike neighbor $\mathbf{x}' \notin \Sigma_\sigma$ (*target voxel*). The proposed change in the lattice configuration (also called *spin flip*) is accepted with a modified family of *Boltzmann transitional probabilities*

(1)

$$
P(\sigma(\mathbf{x}) \to \sigma(\mathbf{x}'))(t) = \begin{cases} p(T_{\Sigma_{\sigma(\mathbf{x})}}(t))e^{-\Delta H|_{\sigma(\mathbf{x})\to\sigma(\mathbf{x}')}/T_{\Sigma_{\sigma(\mathbf{x})}}(t)} \\ \qquad\qquad\qquad\qquad\qquad\quad \Delta H|_{\sigma(\mathbf{x})\to\sigma(\mathbf{x}')} > 0\,; \\ p(T_{\Sigma_{\sigma(\mathbf{x})}}(t)) \qquad\qquad\quad \Delta H|_{\sigma(\mathbf{x})\to\sigma(\mathbf{x}')} \le 0\,, \end{cases}
$$

where $\Delta H|_{\sigma(\mathbf{x})\to\sigma(\mathbf{x}')}$ is the net variation in the total energy of the system as a consequence of the spin update and $T_{\Sigma_{\sigma(\mathbf{x})}} \in \mathbb{R}^+$ is a Boltzmann temperature, which does not reflect any conventional thermal temperature nor correlates to an overall *system motility*, but characterizes each single individual, assuming therefore the role of its specific *intrinsic motility*. $p(T_{\Sigma_\sigma}(t)) : \mathbb{R}^+ \mapsto [0,1]$, a sort of *maximum transition probability*, is a con-

tinuous and increasing function of T_{Σ_σ}, and is characterized by

$$(2) \qquad \begin{cases} p(0) = 0; \\ \lim_{T_{\Sigma_\sigma} \to +\infty} p(T_{\Sigma_\sigma}) = 1. \end{cases}$$

W.r.t. the classical Boltzmann functions used in literature [5,6,10], (1) takes into account of the object motility also in the case of energetically favorable displacement attempts: this allows to consider and realistically reproduce the cases of "frozen" elements, which do not move even if they sense external forces (i.e., resulting in $\Delta H \ll 0$), as commented in [12]. After the discrete object Σ_σ has evolved through a spin flip, both equations that describe the variation of continuous fields, and the attributes of all the objects are rederived, on the basis of new lattice configuration. The basic step of the Metropolis algorithm, called *Monte Carlo Step* (MCS), is then iterated until the end of the simulation time or until the whole system reaches an energetic global minimum, if it exists. A direct correspondence between a MCS and the actual time scale may be therefore not straightforward, giving rise to one of the main criticisms of the method. A realistic correspondence is usually set by fitting *a posteriori* the temporal dynamics of the simulated phenomenon with the relative experimental counterparts.

The *effective energy* of the system, given by the *Hamiltonian H*, contains a variable number of terms, which can be grouped as:

$$(3) \qquad H(t) = H_{adhesion}(t) + H_{constraint}(t) + H_{force}(t).$$

$H_{adhesion}$ describes the adhesive/repulsive interfacial energy between all the couples of discrete objects that interact across their common membrane. $H_{adhesion}$ is based on Steinberg's *Differential Adhesion Hypothesis* (DAH) [6,13]. The DAH proposes that individuals in the same aggregate adhere to each other with different strengths, according to their type. Such a hierarchy of contact forces is one of the main driving mechanisms behind of the evolution of biological systems, whose final organization maximizes the overall strength of interface interactions (or, in other words, minimizes the overall adhesion energy). The typical formulation of DAH-derived $H_{adhesion}$ is:

$$(4) \qquad H_{adhesion}(t) = \sum_{\mathbf{x},\mathbf{x}' \in \Omega_{\mathbf{x}}' : (\partial \mathbf{x} \in \partial \Sigma_\sigma) \cap (\partial \mathbf{x}' \in \partial \Sigma_{\sigma'}) \neq \emptyset} J_{\tau(\Sigma_{\sigma(\mathbf{x})}),\tau(\Sigma_{\sigma'(\mathbf{x}')})}(t),$$

where, as seen, $\mathbf{x}$ and $\mathbf{x}'$ are two neighboring sites and Σ_σ and $\Sigma_{\sigma'}$ the relative two neighboring objects. The coefficients $J_{\tau(\Sigma_\sigma),\tau(\Sigma_{\sigma'})} \in \mathbb{R}$ are the binding forces per unit area, the first type of the so-called Potts parameters,

and are obviously symmetric w.r.t. the indices. In the case of cells, such contact strengths give a qualitative measure of the expression of the different types of adhesion molecules (e.g., integrins or cadherins) characterizing a specific cell line.

The term $H_{constraint}$, whose use also comes from the physics of classical mechanics, sums the energetic components that describe the object attributes. They are written as energetic penalties that increase as the objects deviate from a designed state:

$$(5) \qquad H_{constraint}(t) = \sum_{\Sigma_\sigma} \sum_{i-constraint} \lambda^i_{\Sigma_\sigma}(t) U(a^i_{\Sigma_\sigma}(t), A^i_{\Sigma_\sigma}(t)),$$

where $a^i_{\Sigma_\sigma}(t)$ is the actual and $A^i_{\Sigma_\sigma}(t)$ the target value of the i-attribute of individual Σ_σ, that can vary in time, and $U(a^i_{\Sigma_\sigma}, A^i_{\Sigma_\sigma}) \geq 0$ is a potential with the property that

$$U(A^i_{\eta,\Sigma_\sigma}, A^i_{\eta,\Sigma_\sigma}) = 0.$$

The Potts parameters $\lambda^i_{\Sigma_\sigma} \in \mathbb{R}^+$ take the role of elastic moduli, which determine the weight of the relative energetic constraint, and thus the importance of the relative attribute. Low values of $\lambda^i_{\Sigma_\sigma}$, in fact, allow the discrete unit Σ_σ to deviate more from the configuration that satisfies the constraint. Indeed, since the energetic contributions given in Eq. (5) smoothly decrease to a minimum when the attributes are satisfied, the modified Metropolis algorithm automatically drives any configuration towards one that satisfies the constraints. Among others, the energetic components relative to geometrical attributes of discrete objects, such as their volume and surface, are of particular relevance. In most published CPMs, the author use a simple quadratic potential

$$(6) \qquad U(a^i_{\Sigma_\sigma}(t), A^i_{\Sigma_\sigma}(t)) = \left[a^i_{\Sigma_\sigma}(t) - A^i_{\Sigma_\sigma}(t) \right]^2.$$

However, the form of (6) has the disadvantage that a finite energy is sufficient by a discrete unit to achieve a vanishing value of one of its constraints, for example to shrink a cell to a point, a situation that should be avoided and that would in principle require an infinite energy. For this reason we propose the use of potentials that blow up in the case of $a^i_{\eta,\Sigma_\sigma} \to 0$ as

$$(7) \qquad U(a^i_{\Sigma_\sigma}(t), A^i_{\Sigma_\sigma}(t)) = \left| \frac{a^i_{\eta,\Sigma_\sigma}(t) - A^i_{\eta,\Sigma_\sigma}(t)}{a^i_{\eta,\Sigma_\sigma}(t)} \right|^p,$$

with $p \in \mathbb{R}^+$. In this way, in addition to the just stated advantages, all the components of $H_{constraint}$ are non-dimensional, and thus all the relative Potts coefficients are coherently scaled to units of energy.

The last term in Eq. (3) includes the energetic counterparts of the forces (both effective and generalized) that act on the simulated individuals and are described in the following form:

$$(8) \qquad H_{force}(t) = - \sum_{\mathbf{x} \in \Sigma_\sigma} \sum_{k-force} \mu^k_{\Sigma_{\sigma(\mathbf{x})}}(t)\, \mathbf{F}^k(t) \cdot \mathbf{r_x},$$

where $\mathbf{r_x} = (i_{\mathbf{x}}, j_{\mathbf{x}}, k_{\mathbf{x}})^T$ is the position vector of lattice site $\mathbf{x}$, which is the application point of force $\mathbf{F}^k$, and $\mu^k_{\Sigma_\sigma}$ is the relative Potts parameter, which measures the effective strength of the force on object Σ_σ. The most diffused examples in CPM applications are the forces that are exerted by extracellular chemical substances (which are described as continuous CPM objects) on a population of cells (which are typical discrete objects):

$$(9) \qquad H^{chemical}_{force}(t) = - \sum_{\Sigma_\sigma} \sum_{\mathbf{x} \in \Sigma_\sigma} \mu^{chem}_{\Sigma_{\sigma(\mathbf{x})}}(t) c(\mathbf{x}, t),$$

where $c(\mathbf{x}, t)$ is the concentration of the chemical sensed by cell site $\mathbf{x}$, whose evolution is usually described by a RD equation and the Potts coefficient $\mu^{chem}_{\Sigma_\sigma}$ is, in this case, an effective chemical potential of cell Σ_σ. The net energy difference caused by such a chemical force is:

$$(10) \qquad \Delta H^{chemical}_{force}\big|_{\sigma(\mathbf{x}) \to \sigma(\mathbf{x}')} = \mu^{chem}_{\Sigma_{\sigma(\mathbf{x})}}[c(\mathbf{x}, t) - c(\mathbf{x}', t)],$$

where $\mathbf{x} \in \Sigma_\sigma$ and $\mathbf{x}' \notin \Sigma_\sigma$ are the two neighboring lattice sites randomly selected during the trial update at time t. In particular, $\mu^{chem}_{\Sigma_\sigma} > 0$ yields to a motion up the gradient of c (which is thus a *chemoattractant*), while $\mu^{chem}_{\Sigma_\sigma} < 0$ yields to a motion in the opposite direction (and c is a *chemorepellent*). Moreover, if c is a non-diffusive fixed substrate, Eq. (9) is a representation of a haptotactic force, as in [14].

The importance of each term in the *Hamiltonian* (i.e., of each included biological mechanism) is defined by the magnitude of the relative Potts parameter, which acts as a sort of *penalty coefficient*. It is indeed possible to easily comprehend the importance of each mechanism involved in the simulated phenomenon by only altering the relative Potts parameter, so that the other terms in the *Hamiltonian* scale accordingly. In particular, by equating all the other terms to zero, it is possible to understand whether such a mechanism is individually capable of producing the process of interest, or whether it requires cooperative processes. In this respect, a crucial role in determining the evolution of the system is therefore played by the hierarchy of the Potts coefficients, and not by their exact values. This consideration allows to overcome one of the main limitations of the CPM: given its energetic nature, a direct one-to-one correspondence between Potts parameters

and experimental quantities is not straightforward, being only possible to infer empirical relationships.

2.1. *Nested approach.*

In most CPMs, the Potts parameters are generally static over the whole simulations, or have unrealistic variations. Furthermore, they are usually common for all the objects of the same type, despite their individuality. In order to overcome this issue, we propose the use of a *nested* approach, based on the assumption that the internal state of a biological individual (i.e., the microscopic level) regulates its biophysical properties (described by mesoscopic Potts coefficients) which, as seen, in turn direct its dynamics (described by the relative term in the *Hamiltonian*).

Procedurally, let Σ_σ denote a certain discrete object: we define its internal state vector $\mathbf{s}_{\Sigma_\sigma} \in \mathbb{R}^n$. The length n of $\mathbf{s}_{\Sigma_\sigma}$, defined by the number of internal factors considered in the microscopic model, represents a sort of internal degree of freedom of Σ_σ. Each component $s_{\Sigma_\sigma,l}$, where $l = 1, ..., n$, is typically represented as a continuous object and can be local (i.e., per site) and/or time-dependent (i.e., linked to a specific regulatory pathway, which needs to be modeled, as it will be explained hereafter). Hence, in general, $\mathbf{s}_{\Sigma_\sigma} = \mathbf{s}_{\Sigma_\sigma}(\mathbf{x}, t)$, where $\mathbf{x} \in \Sigma_\sigma$. The spatial localization of $\mathbf{s}_{\Sigma_\sigma}$ is mandatory to accurately represent internal inhomogeneities of Σ_σ, while its time-dependence to reproduce its microscopic evolution. For any Σ_σ, let us consider a generic Potts coefficient $\alpha \in \{\lambda_{\Sigma_\sigma}^i; T_{\Sigma_\sigma}; \mu_{\Sigma_\sigma}^k, ...\}$. We now define $\mathbf{s}_{\Sigma_\sigma}^\alpha \in \mathbb{R}^m$, where $m \leq n$, the subvector of $\mathbf{s}_{\Sigma_\sigma}$ whose components influence the biophysical property of Σ_σ described by α. Therefore the spatio-temporal evolution of α can be expressed as

$$(11) \qquad \alpha(\mathbf{x} \in \Sigma_\sigma, t) = f(\mathbf{s}_{\Sigma_\sigma}^\alpha(\mathbf{x}, t)),$$

where $f : \mathbb{R}^m \mapsto \mathbb{R}$ is a continuous function, which obviously needs to be appropriately defined in relation to the case of interest. According to the same notation, if $\gamma \in \{J_{\tau(\Sigma_\sigma), \tau(\Sigma_{\sigma'})}\}$, for each local interface between neighboring objects (i.e., $\partial\mathbf{x} \in \partial\Sigma_\sigma \cap \partial\mathbf{x}' \in \partial\Sigma_{\sigma'}$ or $\partial\mathbf{x} \in \partial\eta \cap \partial\mathbf{x}' \in \partial\eta'$ in the case of compartmentalized individuals), we have:

$$(12) \quad \gamma((\partial\mathbf{x} \cap \partial\mathbf{x}'), t) = \gamma(\mathbf{s}_{\Sigma_\sigma}^\gamma(\mathbf{x}, t), \mathbf{s}_{\Sigma_{\sigma'}}^\gamma(\mathbf{x}', t)) = g(\mathbf{s}_{\Sigma_\sigma}^\gamma(\mathbf{x}, t), \mathbf{s}_{\Sigma_{\sigma'}}^\gamma(\mathbf{x}', t)),$$

where $g : \mathbb{R}^m \times \mathbb{R}^m \mapsto \mathbb{R}$. The local adhesive strengths are indeed determined by the local internal state of both elements, as they are not only a property of each single individual.

Indeed, the Potts parameters which can locally vary (such as the adhesive interactions or the effective strengths of specific forces) require that

the relative functions of the internal state vector **s** are local (i.e., they need to take into account of the local concentration of the internal factors of interest), whereas the Potts parameters characterizing an entire individual (such as the motility or the elasticity) require that the relative functions of **s** are global (i.e., they need to take into account of the overall level of the internal factor of interest). Summing up, Eqs. (11) and (12) state that the variation of the Potts coefficients of an element (either an entire individual or one of its compartments) is due to the evolution of its internal state: in this way its mesoscopic biophysical properties are no longer given *a priori* (or varied with prescribed rules) but are autonomously and continuously inherited from the flow of information coming from its microscopic level.

The application of the new approach to biological cells is of particular interest. In this context, each component of the internal state vector represents the spatio-temporal variation of the concentration of intracellular ions and molecules, which can be represented as continuous objects and whose quantity regulates the cell phenomenology. In particular, for any component $s_{\Sigma_\sigma, l}$ of $\mathbf{s}_{\Sigma_\sigma}$, given a well-characterized (although simplified) biochemical pathway, it is always possible to set a suitable model (such as a reaction-diffusion (RD) system, which specializes in several coupled differential equations, whose outcome is $s_{\Sigma_\sigma, l}$ itself.

2.2. *Motility of individuals.*

The description of the motility of individuals is one of the most attractive features of the CPM. The Metropolis algorithm is in fact able to represent the exploratory behavior of biological organisms through biased extensions and retractions of their boundaries. It also allows to differentiate the isotropic intrinsic motility of each element, which is described by its Boltzmann temperature T (which can be approximately compared to a diffusion coefficient with a continuous point of view), and the directional, force-based component of its motion. Indeed, since a difference in a potential energy is the work done by a force, for each object Σ_σ we can write

$$(13) \qquad \frac{\Delta H}{\Delta t} = -\prod = -\sum_{\mathbf{x} \in \Sigma_\sigma} \mathbf{F}_{\mathbf{x} \in \Sigma_\sigma} \cdot \frac{\Delta \mathbf{x}}{\Delta t} = -\mathbf{F}_{\mathbf{x} \in \Sigma_\sigma} \cdot \mathbf{v}_{\mathbf{x} \in \Sigma_\sigma},$$

where $\prod$ is the power of force $\mathbf{F}_{\mathbf{x} \in \Sigma_\sigma}$ and $\mathbf{v}_{\mathbf{x} \in \Sigma_\sigma}$ the local velocity. In extremely viscous regimes, such as biological environments, the local force is proportional to the local velocity, and not to the acceleration. This leads to the so-called *overdamped force-velocity response* which is characteristic

of other IBMs [4] and writes

$$(14) \qquad \mathbf{F_{x \in \Sigma_\sigma}} = \alpha_{\mathbf{x} \in \Sigma_\sigma} \mathbf{v_{x \in \Sigma_\sigma}} = \frac{1}{k_{\mathbf{x} \in \Sigma_\sigma}} \mathbf{v_{x \in \Sigma_\sigma}} \propto \frac{1}{p(T_{\Sigma_\sigma}) T_{\Sigma_\sigma}} \mathbf{v_{x \in \Sigma_\sigma}}.$$

As analytically demonstrated in [8,12], the coefficient $k_{\mathbf{x} \in \Sigma_\sigma}$ is the *net rate of transition* of site $\mathbf{x}$ (i.e., the difference between its probability of moving and staying still, $P(\sigma(\mathbf{x}) \to \sigma(\mathbf{x}')) - P(\sigma(\mathbf{x}) \nrightarrow \sigma(\mathbf{x}')))$ and is proportional to the Boltzmann temperature of the element T_{Σ_σ} scaled by the value of $p(T_{\Sigma_\sigma})$. However, w.r.t. those published results, we here prefer to use a proportional dependence and not an equation, since the exact relation between the Monte Carlo spin copy attempts and the continuous time, as well as the kinetics application of the Metropolis-like algorithm, are still debated and a persistent sources of criticism. Putting (14) in (13), we obtain

$$(15) \qquad \frac{\Delta H}{\Delta t} \propto - \sum_{\mathbf{x} \in \Sigma_\sigma} \frac{1}{p(T_{\Sigma_\sigma}) T_{\Sigma_\sigma}} \mathbf{v}^2_{\mathbf{x} \in \Sigma_\sigma} = - \frac{1}{p(T_{\Sigma_\sigma}) T_{\Sigma_\sigma}} \sum_{\mathbf{x} \in \Sigma_\sigma} \mathbf{v}^2_{\mathbf{x} \in \Sigma_\sigma},$$

given that T_{Σ_σ} is a global property of the entire object. Let us now decompose the velocity $\mathbf{v_{x \in \Sigma_\sigma}}$ as

$$(16) \qquad \mathbf{v_{x \in \Sigma_\sigma}} = \mathbf{v}^{CM}_{\Sigma_\sigma} + \mathbf{w_{x \in \Sigma_\sigma}},$$

where $\mathbf{v}^{CM}_{\Sigma_\sigma}$ is the velocity of the object center of mass and $\mathbf{w_{x \in \Sigma_\sigma}}$ a local fluctuation. Simple calculations lead to

$$(17) \quad \sum_{\mathbf{x} \in \Sigma_\sigma} \mathbf{v_{x \in \Sigma_\sigma}} = \sum_{\mathbf{x} \in \Sigma_\sigma} \mathbf{v}^{CM}_{\Sigma_\sigma} + \sum_{\mathbf{x} \in \Sigma_\sigma} \mathbf{w_{x \in \Sigma_\sigma}} = \mathbf{v}^{CM}_{\Sigma_\sigma} a^{volume}_{\Sigma_\sigma} + \sum_{\mathbf{x} \in \Sigma_\sigma} \mathbf{w_{x \in \Sigma_\sigma}},$$

where the second term of the sum vanishes. Therefore, substituting in (13), we obtain

$$(18) \qquad \frac{\Delta H}{\Delta t} \propto - \frac{1}{p(T_{\Sigma_\sigma}) T_{\Sigma_\sigma}} \left[(\mathbf{v}^{CM}_{\Sigma_\sigma})^2 a^{volume}_{\Sigma_\sigma} + \sum_{\mathbf{x} \in \Sigma_\sigma} \mathbf{w}^2_{\mathbf{x} \in \Sigma_\sigma} \right].$$

Given that $\frac{\Delta H}{\Delta t} = \frac{\Delta H}{\Delta \mathbf{x}^{CM}_{\Sigma_\sigma}} \mathbf{v}^{CM}_{\Sigma_\sigma}$, we can finally conclude that

$$(19) \qquad \frac{\Delta H}{\Delta \mathbf{x}^{CM}_{\Sigma_\sigma}} \propto - \frac{1}{p(T_{\Sigma_\sigma}) T_{\Sigma_\sigma}} \left[\mathbf{v}^{CM}_{\Sigma_\sigma} a^{volume}_{\Sigma_\sigma} + \frac{1}{\mathbf{v}^{CM}_{\Sigma_\sigma}} \sum_{\mathbf{x} \in \Sigma_\sigma} \mathbf{w}^2_{\mathbf{x} \in \Sigma_\sigma} \right],$$

or, with another view point,

$$(20) \qquad a^{volume}_{\Sigma_\sigma} \mathbf{v}^{CM}_{\Sigma_\sigma} \propto - p(T_{\Sigma_\sigma}) T_{\Sigma_\sigma} \frac{\Delta H}{\Delta \mathbf{x}^{CM}_{\Sigma_\sigma}} - \frac{1}{\mathbf{v}^{CM}_{\Sigma_\sigma}} \sum_{\mathbf{x} \in \Sigma_\sigma} \mathbf{w}^2_{\mathbf{x} \in \Sigma_\sigma}.$$

Some comments on the consequences of relations (19) and (20):

- they are a definitive confirmation that discrete objects move in order to minimize the total energy;
- the modulus of the velocity of the center of mass of Σ_σ depends on the magnitude of the energy difference due to the proposed spin flip, as well as on its intrinsic motility T_{Σ_σ}, which, in our extended approach, is coherently a variable property of each unit Σ_σ and is determined by its microscopic state: different individuals therefore have different velocities even if they experience the same energy difference;
- it is straightforward to evaluate the contribution to the velocity of unit Σ_σ of each term of the *Hamiltonian*. In fact, for any mechanism i, by equating all the other terms to zero, we obtain:

$$(21) \qquad a_{\Sigma_\sigma}^{volume} \mathbf{v}_{\Sigma_\sigma}^{CM}\big|_{i-mechanism} \propto -p(T_{\Sigma_\sigma})T_{\Sigma_\sigma}\frac{\Delta H^{i-mechanism}}{\Delta \mathbf{x}_{\Sigma_\sigma}^{CM}}.$$

2.3. *Test simulation: in vitro tubulogenesis.*

In order to show how the extended CPM can be applied, and to clarify the complex notation, we here present a model reproducing a classical *tubulogenic* assay. It consists in the autonomous organization of a dispersed population of endothelial cells (ECs) in a bidimensional network, which resembles a primitive *in vivo* capillary-like plexus, see Fig. 2(A). The overall process is mediated by the activity of an autocrine chemical morphogen (such as the VEGF [15]), which not only acts as a chemoattractant but also initiates a series of downstream pathways involving intracellular messengers nitric oxide (NO) and arachidonic acid (AA) and culminating in calcium signals [16,17], Fig. 2(B). The subsequent accumulation of the ion regulates selected biophysical properties of the ECs, such as their motility, adhesive capability, chemotactic strength and elasticity [18].

In the nested environment, we use a CPM to represent the phenomenology of ECs and a continuous method to approach the VEGF-induced calcium-dependent cascades. These levels are interfaced by a set of constitutive relations for the evolution of the Potts coefficients. The ECs are modeled as discrete objects $\Sigma_{\sigma=1,\ldots,200}$ of type $\tau = C$. They reside in an experimental medium, which is represented as a generalized substrate $\Sigma_{\sigma=0}$ of type $\tau = M$. The internal state vector of each cell is

- $\mathbf{s}_{\Sigma_{1,\ldots,200}}(\mathbf{x},t) = (a(\mathbf{x},t), n(\mathbf{x},t), c(\mathbf{x},t)) \in \mathbb{R}^3$,

where $a(\mathbf{x},t)$ corresponds to the local concentration of AA, $n(\mathbf{x},t)$ of NO and $c(\mathbf{x},t)$ of Ca^{2+}. The system *Hamiltonian* is given by:

$$(22) \qquad H(t) = H_{adhesion}(t) + H_{constraint}(t) + H_{chemotaxis}(t).$$

$H_{adhesion}$ considers the intercellular adhesive interactions. In particular, $J_{C,C}$ gives a measure of the formation of local intercellular VE-cadherin-VE-cadherin complexes, which depends on the quantity of active exposed molecules on either sides of the interface. Indeed, since VE-cadherin activity is enhanced by calcium ions, for any cell $\Sigma_{\sigma=1,...,200}$:

- $\mathbf{s}_{\Sigma_\sigma}^J(\mathbf{x}, t) = (c(\mathbf{x}, t))$ and $J_{C,C}((\partial\mathbf{x} \in \partial\Sigma_{\sigma(\mathbf{x})}) \cap (\partial\mathbf{x}' \in \partial\Sigma_{\sigma(\mathbf{x}')}), t) = g(c(\mathbf{x}, t), c(\mathbf{x}', t)) = J_0 \exp\left(-p\, c(\mathbf{x}, t)c(\mathbf{x}', t)\right).$

$H_{constraint}$ takes into account of cell shape changes (i.e., of area and perimeter, since we are in 2D), using potentials of type (7). The target values $A_{\Sigma_{\sigma=1,...,200}}^{surface,perimeter}$ are EC initial dimensions. Cell volume fluctuations are indeed kept negligible by high constant values for $\lambda_{\Sigma_{\sigma=1,...,200}}^{surface} = 20$, whereas the deformability is a characteristic of each cell, being regulated by its intracellular level of calcium. Therefore for each $\sigma = 1, ..., 200$, we set:

- $\mathbf{s}_{\Sigma_\sigma}^{\lambda^{perimeter}}(\mathbf{x}, t) = (c(\mathbf{x}, t))$ and
  $\lambda_{\Sigma_\sigma}^{perimeter}(t) = f(c(\mathbf{x}, t)) = \lambda_0^{per} \exp\left(-k \sum_{\mathbf{x}\in\Sigma_\sigma} c(\mathbf{x}, t)\right).$

Finally, the movement of ECs along gradients of VEGF concentration is implemented by a linear-type chemotaxis term of the form (9):

$$(23) \qquad \Delta H_{chemotaxis} = \mu_{\Sigma_\sigma}^{ch}(\mathbf{x}, t)\left[v(\mathbf{x}, t) - v(\mathbf{x}', t)\right],$$

where the chemical strength is also calcium-dependent. Indeed, for each cell $\Sigma_{\sigma=1,...,200}$, we assume:

- $\mathbf{s}_{\Sigma_\sigma}^{\mu^{chem}}(\mathbf{x}, t) = (c(\mathbf{x}, t))$ and $\mu_{\Sigma_\sigma}^{chem}(\mathbf{x}, t) = f(c(\mathbf{x}, t)) = \mu_0^{ch}\, c(\mathbf{x}, t).$

The cell culture evolves following the Boltzmann probability function (1), with $p = \tanh$. In particular, each cell is characterized by its own variable motility, function of its overall calcium level, as for $\sigma = 1, ..., 200$:

- $\mathbf{s}_{\Sigma_\sigma}^T(\mathbf{x}, t) = (c(\mathbf{x}, t))$ and $T_{\Sigma_\sigma}(t) = f(c(\mathbf{x}, t)) = T_0 \sum_{\mathbf{x}\in\Sigma_\sigma} c(\mathbf{x}, t).$

The evolution of the microscopic variables is regulated by a set of standard

reaction-diffusion equations:

(24)
$$
\begin{cases}
\dfrac{\partial v}{\partial t} = \underbrace{D_v \Delta v}_{diffusion} - \underbrace{\lambda_v v \delta_{\tau(\Sigma_{\sigma(\mathbf{x})}),M}}_{decay} + (\underbrace{\varepsilon_v}_{prod.} - \underbrace{\chi_v v(\mathbf{x},t)}_{uptake}) \delta_{\tau(\Sigma_{\sigma(\mathbf{x})}),C} & \text{in } \mathbf{x} \in \Omega; \\[3mm]
\dfrac{\partial a}{\partial t} = \underbrace{D_a \Delta a}_{diffusion} - \underbrace{\lambda_a a}_{decay} + \underbrace{\varepsilon_a v}_{VEGF-ind.\ prod.} + \underbrace{\epsilon_a c}_{Ca-ind.\ prod.} & \text{in } \mathbf{x} \in \Sigma_{1,\dots,200}; \\[3mm]
\dfrac{\partial n}{\partial t} = \underbrace{D_n \Delta n}_{diffusion} - \underbrace{\lambda_n n}_{decay} + \underbrace{\varepsilon_n v}_{VEGF-ind.\ prod.} + \underbrace{\epsilon_n ca}_{AA-\ and\ Ca-ind.\ prod.} & \text{in } \mathbf{x} \in \Sigma_{1,\dots,200}.
\end{cases}
$$

Notice that the equation of the intracellular messengers AA and NO work only within the ECs. All the coefficients of diffusivity, degradation or decay, and production of the chemicals are constant in time, homogeneous in space and derived from previous experimental determinations [19]. The local concentration of calcium is determined by a balance between the AA- and NO-activated fluxes, its extrusion from the cell cytosol and its buffered diffusion. Its evolution therefore satisfies:

(25)
$$
\begin{cases}
\dfrac{\partial c}{\partial t} = K_{buff} \underbrace{D_c \Delta c}_{diffusion} & \text{in } \mathbf{x} \in \Sigma_{1,\dots,200}; \\[3mm]
n_{\partial \mathbf{x} \in \partial \Sigma_\sigma} \cdot \nabla c = \underbrace{f_a a + f_n n}_{influxes} - \underbrace{f_o c}_{efflux} & \text{at } \partial \mathbf{x} \in \partial \Sigma_{1,\dots,200}; \\[3mm]
\dfrac{\partial c}{\partial t} = \underbrace{D_c \nabla^2 c}_{diffusion} & \text{in } \mathbf{x} \in \Sigma_0,
\end{cases}
$$

where $n_{\partial \mathbf{x}}$ is the unit outward normal to the external boundary of site $\mathbf{x} \in \Sigma_{\sigma=1,\dots,200}$. The coefficient of diffusion, D_c, is assumed to be homogeneous, while the scaling factor $K_{buff} < 1$ models the activity of endogenous buffers (proteins and mitochondria), which bind the ion [20].

The proposed multilevel environment is able to reproduce in close comparison with *in vitro* observations the kinetics of the patterning, as well as its final configuration, see Fig. 2(C). In particular, the ECs organize into a structured network, where cords of cells enclose lacunae. Vascular branches typically are 1-2 cells wide, while lacunae are almost uniform in size (i.e., they range from 120 μm to 150 μm). In particular, such natural length scales are functional and instrumental for an optimal metabolic exchange: a coarser capillary pattern would be in fact unable to differentiate to form the lumen, while an immature and finer structure would be obviously useless [21]. The geometrical description of the emerging structure
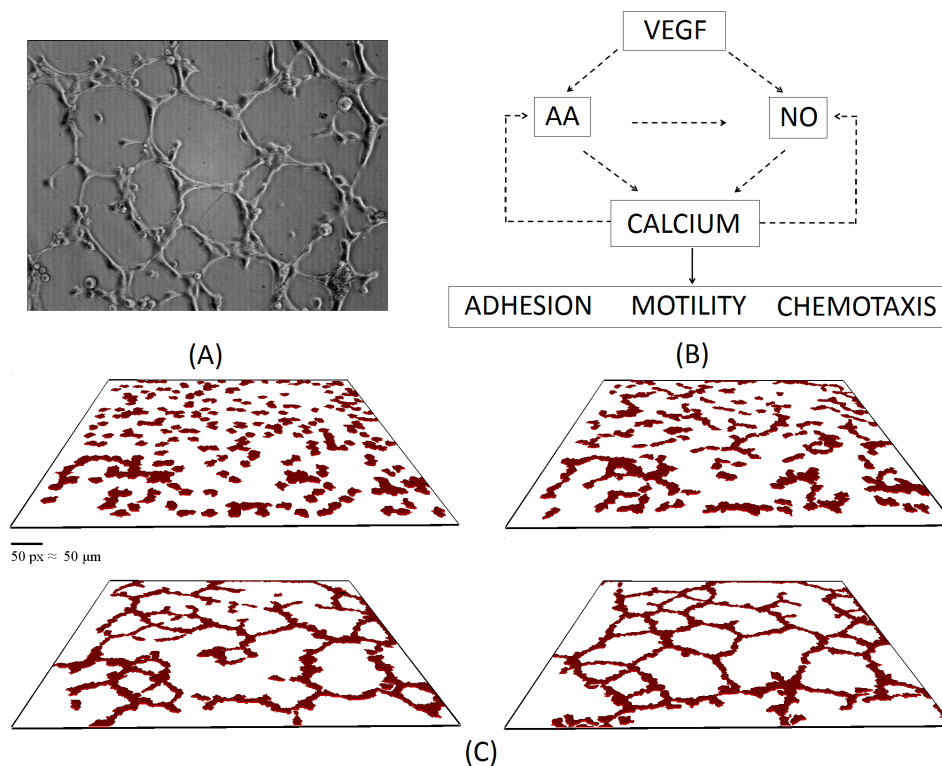
Figure 2. *In vitro* tubulogesis. (A) Experimental image of the final configuration of a HUVEC network. (B) Schematic representation of VEGF-induced calcium-dependent pathways. VEGF activates a series of intracellular events inducing the intracellular production of arachidonic acid (AA) and nitric oxide (NO). Both intracellular messengers are able to activate the entry of extracellular calcium, which, with a feedback mechanism, enhances their biosyntesis. The increment in calcium level triggers cell motility, adhesion, chemical responses and cytoskeletal reorganization. (C) Representative images showing different stages of tubule organization at time intervals of 3 hours.

is in good agreement with experimental analysis provided on cultures of human breast carcinoma-derived ECs (B-TECs, [16]) and human umbilical vein ECs, (HUVECs, [19]). The pattern formation is realistically driven by the complex and coordinated interplay of multiscale mechanisms, i.e. the calcium-dependent increase in cell motility, adhesion and cytoskeletal remodeling and the VEGF-mediated chemotactic migration.

3. Compartmentalization approach.

Most CPM models, as the one presented above, represent discrete object as isotropic objects, formed by equivalent and undifferentiated sites. This representation provides a useful level of abstraction, but also hides relevant

inhomogeneous properties that characterize all biological individuals and are important to keep in several applications. For example, in the case of cells, the cytoskeleton, the plasmamembrane, the nucleus and other internal organelles are not distinguished.

The simplest and most realistic way of reproducing such complex morphologies is to introduce a *compartmentalization* technique. According to this approach, a collection of standard CPM objects can be clustered to form a compartmentalized element, which can more accurately reproduce a real individual. In other words, if in the basic CPM a single discrete object represented an entire individual, it now represents one of its compartments. Technically, with the new procedure, the discrete units Σ_σ share an additional attribute, a cluster id $\eta(\Sigma_\sigma) \in \mathbb{N}$, which defines the compartmentalized individual they belong to. Obviously, discrete units without η are not part of a compartmentalized entity, but represent, on their own, an entire element (as in the basic CPM). Apart from the type already defined for the discrete units, $\tau(\Sigma_\sigma)$, we can now introduce a type for the entire clusters, $\theta(\eta)$. The borders between subunits belonging to the same individual represent internal membranes, while its external membrane is defined as $\partial\eta = \bigcup_{\mathbf{x}\in\Sigma_\sigma\subseteq\eta,\mathbf{x}'\in\Omega'_\mathbf{x}:\mathbf{x}'\in\Sigma_{\sigma'}\nsubseteq\eta}(\partial\mathbf{x} \cap \partial\mathbf{x}')$. Here and in the following, we will use the simplified notations $\mathbf{x} \in \eta$ to identify a site $\mathbf{x}$ belonging to a compartmentalized individual η (i.e., it would write $\mathbf{x} \in \Sigma_\sigma \subseteq \eta$) and $\partial\mathbf{x} \in \partial\eta$ to identify that $\partial\mathbf{x}$ belongs to the external membrane of η.

The new representation of individuals requires a redefinition of the characteristic terms of the CPM. First, it is necessary to differentiate the contributions of $H_{adhesion}$ due either to the contact between couples of discrete units belonging to the same element, namely $H^{int}_{adhesion}$, or to the contact between the membranes of couples of units belonging to different elements, namely $H^{ext}_{adhesion}$:

$$(26) \qquad H_{adhesion}(t) = H^{int}_{adhesion}(t) + H^{ext}_{adhesion}(t).$$

$H^{int}_{adhesion}$, which indeed models contact forces within the same individual (e.g. between the nucleus and the cytosol in a cell), writes as
(27)
$$H^{int}_{adhesion}(t) = \sum_{\substack{\mathbf{x},\mathbf{x}'\in\Omega'_\mathbf{x}: \\ (\partial\mathbf{x}\in\partial\Sigma_\sigma)\cap(\partial\mathbf{x}'\in\partial\Sigma_{\sigma'})\neq\emptyset}} J^{int}_{\tau(\Sigma_{\sigma(\mathbf{x})}),\tau(\Sigma_{\sigma'(\mathbf{x}')})}(t)\delta_{\eta(\Sigma_{\sigma(\mathbf{x})}),\eta(\Sigma_{\sigma'(\mathbf{x}')})}(t).$$

The form of Eq. (27) is analogous to that of Eq. (4) and δ is the Kronecrete delta. $J^{int}_{\tau(\Sigma_\sigma),\tau(\Sigma_{\sigma'})} \in \mathbb{R}^-$ account for high contact tensions, which prevent single individuals from splitting, as commented in [22].

$H^{ext}_{adhesion}$ is formed instead by the effective adhesion energies between different compartmentalized individuals, that interact with their external

membranes:

$$(28) \qquad H_{adhesion}^{ext}(t) = \sum_{\mathbf{x},\mathbf{x}' \in \Omega_{\mathbf{x}}':(\partial\mathbf{x}\in\partial\eta)\cap(\partial\mathbf{x}'\in\partial\eta')\neq\emptyset} J_{\theta(\eta),\theta(\eta')}^{ext}(t).$$

The strengths $J_{\theta(\eta),\theta(\eta')}^{ext} \in \mathbb{R}^+$ depend, as a simple extension of the basic CPM, on the types of the respective interacting clusters. It is worth to notice that, if the objects in contact represent standard non-compartmentalized individuals, the relative energetic contributions are in the classical form of Eq. (4).

The compartmentalized approach requires then to specify both the attributes and the experienced forces (i.e., and the relative energetic contributions) for each and every subunit that formed the compartmentalized individuals. Although a simulated element can in principle be compartmentalized in a variety of ways (for example, along symmetry planes, or in a fixed number of equivalent and undifferentiated subunits), a biologically plausible compartmentalization is obviously preferable. Indeed, the compartmentalized approach is clearly flexible, since it allows the level of details to be tuned by only increasing or decreasing the number of units that form a clustered individual, or the number of lattice sites per functional unit.

Finally, the specific microscopic models of intracellular dynamics can be used together with the compartmentalized approach described in the previous section (if Σ_σ represents a subregion of a compartmentalized individual η, the internal state vector is $\mathbf{s}_{\eta,\Sigma_\sigma}$). The biochemical processes can in fact be localized within a well-defined subcellular compartment, as occurs in reality, allowing to handle several biological mechanisms, which are difficult to reproduce with the basic CPM.

3.1. *Test simulation: cell movement in a fibrous matrix.*

In order to provide the usefulness of the compartmentalization approach, we model the migration of an individual cell within a dense fibrous scaffold. The cell, initially a sphere, is differentiated in two compartments: the central nucleus ($\Sigma_{\sigma=1}$, $\tau(\Sigma_{\sigma=1}) = N$) and the surrounding cytosol ($\Sigma_{\sigma=2}$, $\tau(\Sigma_{\sigma=2}) = C$), see Fig. 3(A, right panel). The cell cluster id is $\eta = 1$, of type $\theta(\eta) = E$. The extracellular environment is composed of a network of 125 collagenous fibers, which are standard, non compartmentalized, CPM objects $\Sigma_{\sigma=3,\ldots,125}$, of type $\tau(\sigma) = F$, and of a special generalized object ($\Sigma_{\sigma=0}$, $\tau(\sigma) = M$), which represents the extracellular medium, homogenously distributed throughout the simulation domain. The matrix threads form a regular cubic mesh characterized by pores of subnuclear dimensions, see again Fig. 3(A, left panel).

The *Hamiltonian H* is formed by two terms. $H_{adhesion}$ is differentiated as in Eq. (26) in the contribution due to either the generalized contact tension between the nucleus and the cytoplasm within the cell, or the effective adhesion between a cell and a matrix component. $J_{N,C}^{int} \ll 0$ implicitly models the forces exerted by intermediate actin filaments and microtubules to anchor the nucleus to the cell cytoskeleton. $J_{E,F}^{ext}$ and $J_{E,M}^{ext}$ are instead a measure of the affinity between cell surface adhesion complexes (i.e. sugar-binding receptors or integrins) to either non-solid (i.e. glycosaminoglycans in medium) or solid (i.e. fibrillar collagen) extracellular ligands, respectively: indeed, we assume $J_{E,F}^{ext} < J_{E,M}^{ext}$ since most cell lines in standard conditions adhere more strongly with the fibrous part of the extracellular matrix rather than with its soluble component.

$H_{constraint}$ models the geometrical attributes of the simulated objects (both the cell subunits and the matrix threads) where the target values $A_{\Sigma_{1,\ldots,125}}^{volume}$ and $A_{\Sigma_{1,\ldots,125}}^{surface}$ are their initial dimensions. Indeed, assuming that the cell does not significantly grow during migration, the fluctuations of their volumes are kept negligible with high constant values of $\lambda_{1,\Sigma_{1,2}}^{volume}$. Moreover, cells moving in matrix environments are typically deformable, but their nuclei show a higher rigidity w.r.t. the cytoplasm region: therefore, we set $\lambda_{1,\Sigma_2}^{surface} < 1$ and $\lambda_{1,\Sigma_1}^{surface} \gg 1$. The matrix fibers are instead assumed inelastic by high $\lambda_{\Sigma_{3,\ldots,125}}^{volume} = \lambda_{\Sigma_{3,\ldots,125}}^{surface} \gg 1$.

Given the *Hamiltonian*, the evolution of the system is driven by the Boltzmann probability function (1), with $p = \tanh$. In particular, the temperature T is assumed to characterize each single object: indeed, T_{1,Σ_1} is a low value reproducing the passive motion of the nucleus, which, unable to have an autonomous movement, is dragged by the surrounding cytosol, characterized instead by a high $T_{1,\Sigma_2} \gg 1$ (that gives a measure of the "real" cell intrinsic motility, i.e. the frequency of cell PM ruffles). Finally, the collagenous threads are fixed by $T_{\Sigma_{3,\ldots,125}} = 0$.

The analysis of cell movement (captured in a time span of 9 hours) shows that any cell migration over long distances is prohibited. An even complete stretch of cell cytosol is in fact not sufficient to pass through the steric hindrances, as the nucleus can not significantly deform, causing the overall individual to be confined in a small area, see Fig. 3(B, left panel). Interestingly, an enhancement in the elasticity of the nuclear cluster, with a low value of $\lambda_{1,\Sigma_1}^{surface}$, results in an appreciable cell movement in such a dense matrix, as the cell is allowed to completely squeeze and stretch through the existing mesh, as captured in Fig. 3(B, right panel) and in the inset therein. It is straightforward to notice that these considerations would have not been pointed out by the basic, non-compartmentalized CPM.
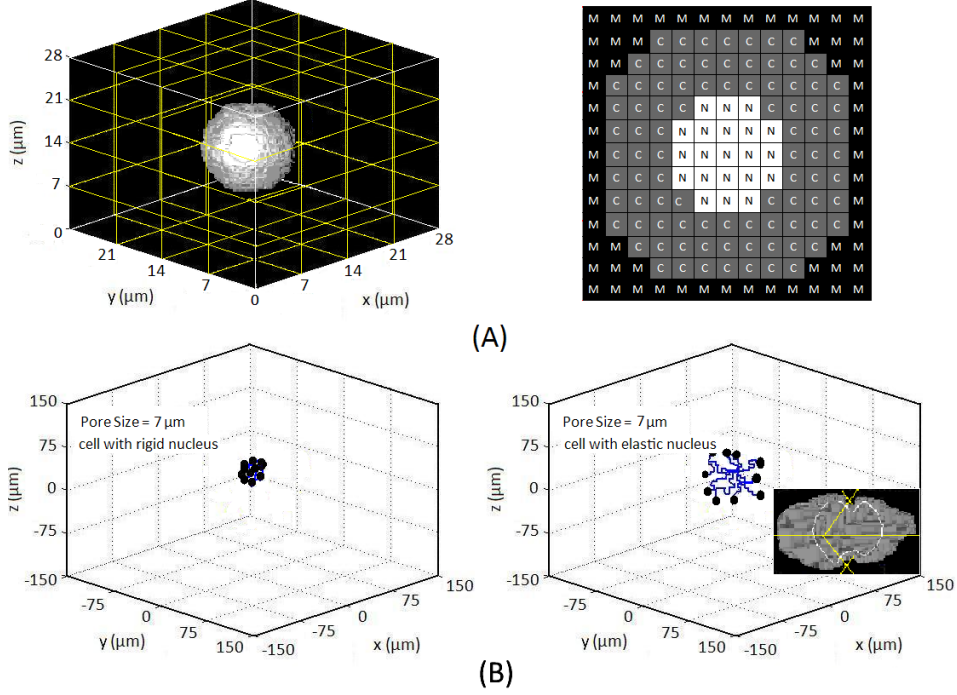
Figure 3. Migration of a single compartmentalized cell within a fibrous matrix. (A, left panel) Domain Ω, a $20 \times 20 \times 20$ lattice (1 lattice site $\approx 4\ \mu m^3$). The cell is initially a 16.5 μm-diameter sphere, with a nucleus with a diameter of 7.5 μ. The fibers are standard objects, 28 μm long and 1.5 μm width, which form a network with subnuclear dimensions (7 μm). (A, right panel) xy section of the compartmentalized cell. It is possible to see the different subunits: the nucleus (Σ_1, $\tau(\Sigma_1) = N$) and the cytosol (Σ_2, $\tau(\Sigma_2) = C$). (B) Wind-rose graphs show 10 cell tracks over 9 h. Cell movement is only permitted by an enhancement in nucleus elasticity. In the inset, the nucleus deforms to allow the entire individual to pass though the dense fiber network. The nucleus is encircled manually. Values of the parameters: $J_{N,C}^{int} = -20$, $J_{E,F}^{ext} = 4$, $J_{E,M}^{ext} = 8$ $\lambda_{1,\Sigma_1}^{vol} = \lambda_{1,\Sigma_2}^{vol} = \lambda_{\Sigma_{3,\dots 125}}^{vol} = \lambda_{\Sigma_{3,\dots,125}}^{surf} = 20$, $\lambda_{1,\Sigma_2}^{surf} = 0.5$; $T_{1,\Sigma_1} = 0.5$, $T_{1,\Sigma_2} = 15$, $T_{\Sigma_{3,\dots,125}} = 0$. $\lambda_{1,\Sigma_1}^{surf}$ is varied from 20 to 1 to model the enhanced nucleus elasticity.

4. Conclusions.

Over the last decade, the CPM method has become a standard technique for cell-to-tissue level *in silico* biology, first replicating, then guiding *in vitro* experiments, and eventually leading to new experimental discoveries [8,23,24]. We have here discussed some improvements of the method, which aim at overcoming its main limitations. Along the text, we have also illustrated some sample simulations, i.e. of a typical tubulogenic assay and of the migration of an individual cell within a dense fibrous scaffold. In both cases, the results obtained by the model have agreed with the pub-

lished experimental observations, thus showing the consistency of our CPM extensions.

REFERENCES

1. M. S. Alber, M. A. Kiskowsky, J. A. Glazier, and Y. Jang, On cellular automation approaches to modeling biological cells, in *Mathematical Systems Theory in Biology, Communication and Finance* (J. Rosenthal and D. S. Gilliam, eds.), pp. 1–40, Springer-Verlag, 2004.

2. A. R. A. Anderson, M. A. J. Chaplain, and K. A. Rejniak, *Single-Cell-Based Models in Biology and Medicine.* Birkaüser, 2007.

3. H. M. Byrne, M. R. Owen, T. Alarcon, J. Murphy, and P. K. Maini, Modelling the response of vascular tumours to chemotherapy: a multi-scale approach, *Math. Mod. Meth. in Appl. Sci.*, vol. 16, no. 7, pp. 1219–1241, 2006.

4. D. Drasdo and S. Hohme, Individual-based approaches to birth and death in avascular tumors, *Math. Comp. Model.*, vol. 37, no. 11, pp. 1163–1175, 2003.

5. J. A. Glazier and F. Graner, Simulation of the differential adhesion driven rearrangement of biological cells, *Phys. Rev. E Stat. Phys. Plasmas Fluids Relat. Interdiscip. Topics*, vol. 47, pp. 2128–2154, 1993.

6. F. Graner and J. A. Glazier, Simulation of biological cell sorting using a two dimensional extended potts model, *Phys. Rev. Lett.*, vol. 69, no. 13, pp. 2013–2017, 1992.

7. A. Balter, R. M. H. Merks, N. J. Poplawski, M. Swat, and A. J. Glazier, The glazier-graner-hogeweg model: extensions, future directions, and opportunities for further study, in *Single-Cell-Based Models in Biology and Medicine* (A. R. A. Anderson, M. A. J. Chaplain, and K. A. Rejniak, eds.), Mathematics and Biosciences in Interactions, pp. 151–167, Birkaüser, 2007.

8. J. A. Glazier, A. Balter, and N. J. Poplawski, Magnetization to morphogenesis: a brief history of the glazier-graner-hogeweg model, in *Single-Cell-Based Models in Biology and Medicine* (A. R. A. Anderson, M. A. J. Chaplain, and K. A. Rejniak, eds.), Mathematics and Biosciences in Interactions, pp. 79–106, Birkaüser, 2007.

9. E. Ising, Beitrag zur theorie des ferromagnetismus, *Z. Physik.*, vol. 31, p. 253, 1925.

10. R. B. Potts, Some generalized order-disorder transformations, *Proc. Camb. Phil. Soc.*, vol. 48, pp. 106–109, 1952.

11. N. Metropolis, A. Rosenbluth, M. N. Rosenbluth, A. H. Teller, and E. Teller, Equation of state calculations by fast computing machines, *J. Chem. Phys.*, vol. 21, no. 6, pp. 1087–1092, 1953.

12. M. Scianna and L. Preziosi, Multiscale developments of the cellular potts model, *Multiscale Model. Simul.*, vol. 10, no. 2, pp. 342–382, 2012.

13. M. S. Steinberg, Does differential adhesion govern self-assembly processes in histogenesis? equilibrium configurations and the emergence of a hierarchy among populations of embryonic cells, *J. Exp. Zool.*, vol. 173, no. 4, pp. 395–433, 1970.

14. S. Turner and J. A. Sherratt, Intercellular adhesion and cancer invasion: a discrete simulation using the extended potts model, *J. Theor. Biol.*, vol. 216, no. 1, pp. 85–100, 2002.

15. P. Carmeliet, Vegf as a key mediator of angiogenesis in cancer, *Oncology*, vol. 69, pp. 4–10, 2005.

16. A. F. Pla, C. Grange, S. Antoniotti, C. Tomatis, A. Merlino, B. Bussolati, and L. Munaron, Arachidonic acid-induced ca2+ entry is involved in early steps of tumor angiogenesis, *Mol. Cancer Res.*, vol. 6, pp. 535–545, 2008.

17. A. Mottola, S. Antoniotti, D. Lovisolo, and L. Munaron, Regulation of noncapacitative calcium entry by arachidonic acid and nitric oxide in endothelial cells, *FASEB J.*, vol. 19, pp. 2075–2077, 2005.

18. M. Scianna, L. Munaron, and L. Preziosi, A multiscale hybrid approach for vasculogenesis and related potential blocking therapies, *Prog. Biophys. Mol. Biol.*, vol. 160, no. 2, pp. 450–462, 2010.

19. G. Serini, D. Ambrosi, E. Giraudo, A. Gamba, L. Preziosi, and F. Bussolino, Modeling the early stages of vascular network assembly, *EMBO J.*, vol. 22, pp. 1771–1779, 2003.

20. P. Bayley, P. Ahlstrom, S. R. Martin, and S. Forsen, The kinetics of calcium binding to calmodulin: Quin 2 and ans stopped-flow fluorescence studies, *Biochem. Biophys. Res. Commun.*, vol. 120, pp. 185–191, 1984.

21. P. D. Chilibeck, D. H. Paterson, D. A. Cunningham, A. W. Taylor, and E. G. Noble, Muscle capillarization o2 diffusion distance, and vo2 kinetics in old and young individuals, *J. Appl. Physiol.*, vol. 82, pp. 63–69, 1997.

22. N. B. Ouchi, J. A. Glazier, J. P. Rieu, A. Upadhyaya, and J. Sawada, Improving the realism of the cellular potts model in simulations of biological cells, *Physica A*, vol. 329, no. 3-4, pp. 451–458, 2003.

23. A. F. M. Marée and P. Hogeweg, How amoeboids self-organize into a fruiting body: multicellular coordination in dictyostelium discoideum, *Proceedings of the National Academy of Sciences of the USA*, vol. 98, pp. 3879–3883, 2001.

24. R. M. H. Merks and P. Koolwijk, Modeling morphogenesis in silico and in vitro: towards quantitative, predictive, cell-based modeling, *Math. Model. Nat. Phenom.*, vol. 4, no. 4, pp. 149–171, 2009.